Image charge effect on two-dimensional excitons in an inorganic-organic quantum-well crystal

Kenichiro Tanaka,* Takayuki Takahashi, and Takashi Kondo
Department of Materials Science, The University of Tokyo, 7-3-1 Hongo, Bunkyo-ku, Tokyo 113-8656, Japan

Tsutomu Umebayashi and Keisuke Asai
Department of Quantum Engineering and Systems Science, The University of Tokyo, 7-3-1 Hongo, Bunkyo-ku, Tokyo 113-8656, Japan

Kazuhiro Ema
Department of Physics, Sophia University, 7-1 Kioi-cho, Chiyoda-ku, Tokyo 102-8554, Japan
(Received 26 July 2004; published 13 January 2005)

We report a clear experimental evidence of the image charge effect on excitons in the optical and electroabsorption spectra of an inorganic-organic quantum-well crystal $(C_6H_{13}NH_3)_2PbI_4$. The *ns* ($n \geqslant 2$) Wannier series are ideal two-dimensional excitons whose binding energies are enhanced by both the spatial confinement and image charge effects. Exceptionally large binding energy of the 1*s* exciton (361 meV) is also due to the prominent image charge effect. We also observed unique blueshifts of the 1*s* excitons under the electric field perpendicular to the quantum-well layers, for which we demonstrated with calculations that the image charge effect plays a significant role.

DOI: 10.1103/PhysRevB.71.045312 PACS number(s): 78.20.Jq, 71.35.Cc, 78.67.De

I. INTRODUCTION

When excitons are confined in low-dimensional systems, they have enhanced binding energies and oscillator strength. For example, it has been theoretically shown that the spatial confinement in an ultrathin and deep quantum well (QW) quadruples the exciton binding energies and halves the exciton Bohr radius.[1] Additionally, it has been theoretically predicted that, if the dielectric constant of the barrier layers is much smaller than that of the well layers, the effective Coulomb interaction between electron and hole in the well layer will be enhanced, resulting in the enhanced excitons binding energies. To our knowledge, however, the clear experimental evidence on this so-called image charge effect[2,3] is quite limited, mainly because the difference of dielectric constants between adjoining layers is not so large in conventional artificial semiconductor nanostructures such as GaAs/$Al_xGa_{1-x}As$ (usually of the order of 10%), so that this effect remains relatively minor effect. Although Kulik *et al.* have reported that the binding energies of the excitons in near-surface $In_xGa_{1-x}As$/GaAs QW is enhanced by the large dielectric constant difference between the QW and the vacuum, the reported enhancement factor of the excitons binding energy due to the image charge effect is still not so large ($\sim$1.5).[4]

On the other hand, when electric fields are applied perpendicular to the QW layers, exciton peaks usually exhibit redshifts (quantum-confined Stark effect QCSE[5]). The mechanism of the QCSE is essentially different from the Stark effect in atoms; QCSE is caused by the band-gap redshifts whose magnitudes exceed the reduction of exciton binding energy due to the field-induced separation of electron and hole. Although the image charge effect can affect the electric-field-induced shifts of excitons in GaAs/$Al_xGa_{1-x}As$ QWs, the contribution remains minor.[6]

An inorganic-organic QW crystal $(C_6H_{13}NH_3)_2PbI_4$ is a self-organized crystal, in which the excitons are tightly confined in the inorganic monomolecular layer of $[PbI_6]$ octahedra ($\sim$6.37 Å) sandwiched between organic barrier layers consisting of alkyl-ammonium chains $[C_6H_{13}NH_3]$ ($\sim$9.97 Å).[7,8] The crystal structure is shown in the inset in Fig. 2. Recently, this crystal has been attracting much interest because it exhibits many fascinating characteristics due to its unique crystal structure, such as huge optical nonlinearity with ultrafast response,[9–11] bright electroluminescence,[12] and outstanding scintillation[13] characteristics. In this crystal, the band gap of the barrier layer is at least 3 eV larger than that of the well layer, and the interfaces between the well and the barrier layer are intrinsically flat; thus this crystal has been considered as an ideal two-dimensional (2D) system. In fact, we have shown recently that the excitons in this crystal are Wannier-type ones with comparatively strong 2D characters.[14] In addition, this crystal has been considered to be a rare system where one may observe explicitly the image charge effect on excitons,[3,15–17] because the difference of the dielectric constants between the adjoining layers is exceptionally large (the dielectric constants of the well and the barrier are about 6.1 and 2.1, respectively[7]) compared with the conventional semiconductor QW structures.

We have found that excitons in this crystal are nearly ideal 2D Wannier excitons whose binding energies are exceptionally large. We have also observed unique blueshift of the 1*s* excitons under the electric field perpendicular to the QW layers, in clear contrast with the QCSE. The purpose of this paper is to show that both the strong 2D spatial confinement and image charge effects play important roles in these unique results.

The structure of this paper is as follows. In Sec. II, the sample preparation and the experimental procedure are briefly described. Results of the reflection and electroabsorption measurements are presented in Sec. III. In Sec. IV, we discuss the effects of the spatial confinement and the image charge enhancement on the exciton characters. Finally, a conclusion is given in Sec. V.

II. EXPERIMENT

We prepared single crystals of $(C_6H_{13}NH_3)_2PbI_4$ in the following procedure. We first prepared $C_6H_{13}NH_3I$ by reaction of $C_6H_{13}NH_2$ with a stoichiometric amount of HI aqueous solution at room temperature. The obtained solution was evaporated to remove water and washed with diethylether until the powder became white. The obtained $C_6H_{13}NH_3I$ was mixed with a stoichiometric amount of PbI_2 in acetone. $(C_6H_{13}NH_3)_2PbI_4$ powder was precipitated by adding nitromethane to the obtained solution. Single crystals of $(C_6H_{13}NH_3)_2PbI_4$ were grown by solvent evaporation from its acetone/nitromethane solution. Controlled slow evaporation (typically for one month) enabled us to obtain very high-quality crystals of $(C_6H_{13}NH_3)_2PbI_4$.

The reflection spectra of $(C_6H_{13}NH_3)_2PbI_4$ single crystals were measured at 5 K over a wide range from 1.5 eV to 5.5 eV. Light from a xenon lamp monochromated with a spectroscope (Acton Research Corp., SP-300i) was focused onto the sample after passing through a polarizer. The reflected light from the sample was detected using a photomultiplier tube (Hamamatsu Photonics Corp., R955). The Kramers-Kronig procedure was used to transform the reflection spectra to absorption spectra.

Electroabsorption (EA) measurements were carried out at 5 K on 200-nm-thick polycrystalline films of $(C_6H_{13}NH_3)_2PbI_4$, where the electric fields are applied perpendicular to the quantum-well layers. Since they are highly oriented with *c* axis perpendicular to the substrate surfaces, their optical properties are almost identical to those of single crystalline sample as measured with normal incidence. The ac electric fields with no dc bias were applied with a frequency of 1 kHz. The sample was a $(C_6H_{13}NH_3)_2PbI_4$ polycrystalline film spin coated on an ITO-deposited glass substrate, onto the top of which a gold electrode was deposited. The modulated electric fields were applied between the ITO and gold electrode. The sample was mounted on a sample holder in a cryostat evacuated to 10^{-5} Torr and maintained at 5 K. Light from a xenon lamp monochromated with a spectroscope was focused onto the sample and the transmitted light was detected with a photomultiplier tube. The transmitted light has dc and ac components which are proportional to the transmission T and the modulated ΔT, respectively. The dc components were measured with a digital multimeter, while the ac components were decomposed with a lock-in amplifier (NF Corp., 5610B) synchronized at twice the field modulation frequency. We have confirmed that there was no electroluminescence in the modulated signals by checking the modulated signals when the light was blocked off. The EA spectra were obtained by calculating $-\Delta T/T$ at each wavelength.

III. RESULTS

Figure 1(a) shows the reflection spectrum of a $(C_6H_{13}NH_3)_2PbI_4$ single crystal for $k\|c$, $E\perp c$, and $E\|a$ configuration at 5 K, where k and E are the wave vector, the polarization vector of the light, respectively, and the *c* axis is perpendicular to the *ab* plane (well plane). Since this crystal has very small anisotropy in the *ab* plane,[7,8] the reflection spectrum for the $E\|a$ configuration is almost identical with that for $E\|b$ (not shown).

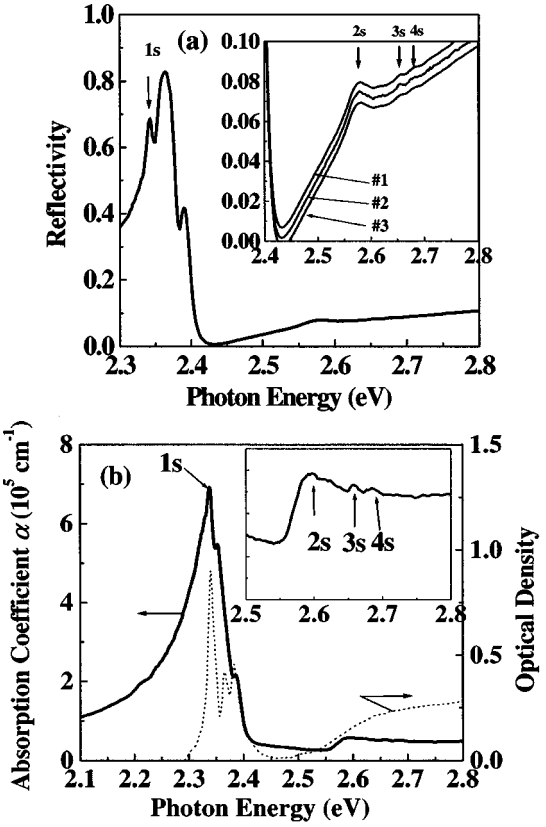

FIG. 1. (a) Reflection spectrum of a $(C_6H_{13}NH_3)_2PbI_4$ single crystal at 5 K. The inset shows the expansion around 2.6 eV, in which the spectra of three different samples (Nos. 1–3) are shown. The reflection spectra for the samples Nos. 2 and 3 are shifted vertically in order for them to be distinguishable. (b) Solid line shows the optical absorption spectrum of a $(C_6H_{13}NH_3)_2PbI_4$ single crystal at 5 K obtained from the Kramers-Kronig transformation of its reflection spectrum. The inset shows the expansion around 2.6 eV. Dotted line shows the optical absorption spectrum of $(C_6H_{13}NH_3)_2PbI_4$ polycrystalline film measured at 5 K (Ref. 14).

The reflectivity peak of the 1*s* exciton (marked as "1*s*") and associated phonon sidebands were clearly observed around 2.34 eV, and steplike structures were also observed around 2.6 eV. The inset in Fig. 1(a) shows the expansion around 2.6 eV. We have found a weaker but distinct peak around 2.595 eV (marked as "2*s*"), which had been attributable to the 2*s* exciton in our previous report.[14] Above them, two weak but distinct peaks have been newly observed. We have confirmed the reproducibility of these structures by measuring three different samples [see the inset in Fig. 1(a)]. The structure around 2.66 eV is attributable to the 3*s* exciton because it is located close to the 3*p* exciton observed in the two-photon absorption spectrum,[14] and the structure just above the 3*s* exciton is to the 4*s* exciton.

Figure 1(b) shows the optical absorption spectrum of $(C_6H_{13}NH_3)_2PbI_4$ at 5 K derived from Kramers-Kronig transformation of its reflection spectrum. The resonance energies of the 1*s*, 2*s*, 3*s*, and 4*s* excitons are 2.339 eV, 2.595

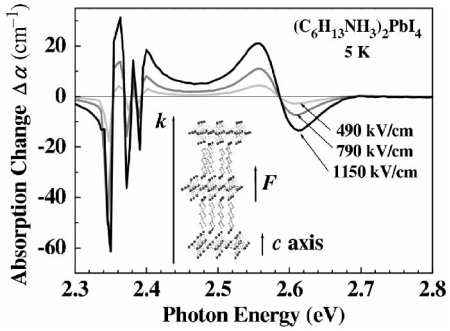

FIG. 2. Electroabsorption spectra of $(C_6H_{13}NH_3)_2PbI_4$ under electric fields perpendicular to the well layers measured at 5 K. The inset shows the crystal structure of $(C_6H_{13}NH_3)_2PbI_4$ with the wave vector of light (k), the applied electric field (F), and the c axis.

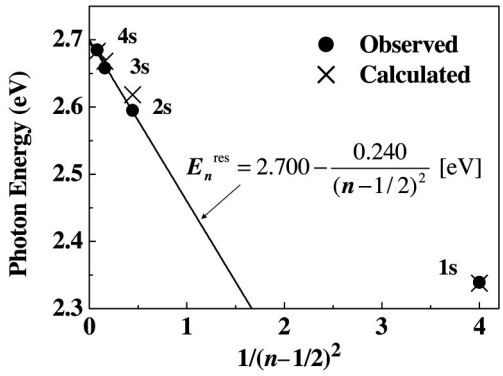

FIG. 3. Resonance energies of Wannier-series excitons in $(C_6H_{13}NH_3)_2PbI_4$ as a function of $1/(n-1/2)^2$. Closed circles and crosses represent the observed and calculated energies of the excitons, respectively. The solid line shows the fitting based on a simple two-dimensional Wannier exciton model.

eV, 2.658 eV, and 2.685 eV, respectively. Although the asymmetricity in the shape of the 1s exciton peak might be an artifact caused in our Kramers-Kronig transformation procedure, the resonance energies of the excitons are highly reliable because the obtained energies of the 1s exciton and its phonon sideband humps agree well with those determined from the absorption spectra measured in polycrystalline thin films of $(C_6H_{13}NH_3)_2PbI_4$ [a typical spectrum is shown by the dotted line in Fig. 1(b)]. In addition, the resonance energy of the 2s excitons determined from our EA study[14] agrees well with that determined here. Therefore, we conclude that the resonance energies determined by the Kramers-Kronig-transformed absorption spectrum are sufficiently accurate, and in the following part of this paper, we thus discuss the exciton structures based on the obtained exciton resonance energies.

Figure 2 shows EA spectra of $(C_6H_{13}NH_3)_2PbI_4$ under electric fields perpendicular to the QW layers. The inset in Fig. 2 is a sketch of the wave vector of light (k), the applied electric field (F), and the crystal structure of $(C_6H_{13}NH_3)_2PbI_4$.

IV. DISCUSSIONS

A. Excitons binding energies

The observed resonance energies of the ns (n principal number) excitons are plotted as a function of $1/(n-1/2)^2$, which are shown by the closed circles in Fig. 3. The observed resonance energies $E_n^{\rm res}$ of the ns ($n \geqslant 2$) excitons are well described by a simple 2D hydrogenic model[1] given by

$$E_n^{\rm res} = 2.700 - 0.240/(n-1/2)^2 \ ({\rm eV}), \qquad (1)$$

indicating that they are ideal 2D Wannier excitons. This is reasonable because their inplane Bohr radii are far larger than the well width. From Eq. (1), the band-gap energy is determined to be 2.700 eV. Therefore, the binding energy of the 1s exciton is 361 meV. As is readily seen in Fig. 3, the 1s exciton resonance energy is deviated to the higher energy side of this formula. Since the so-called central cell correction usually makes 1s excitons deviate to the lower energy side from the simple hydrogenic model[18], the observed deviation is unusual. The observed smaller binding energy of the 1s exciton is a result of the following two factors: (1) Since the in-plane Bohr radius of the 1s exciton is not much larger than the well width, the spatial confinement effect on the 1s exciton is not so sufficient compared to that on the ns ($n \geqslant 2$) excitons. (2) The relatively small Bohr radius of the 1s exciton results also in weaker penetration of the line of electric force between the electron and the hole into barrier layers with lower dielectric constant, and thus leads to smaller enhancement due to the image charge effect in contrast to very large enhancement on ns ($n \geqslant 2$) excitons.

To analyze quantitatively, we calculated the ns excitons binding energies E_n^b based on Muljarov's formalism.[16] We solved a 2D Schrödinger equation describing the in-plane exciton motion

$$-\frac{\hbar^2}{2\mu}\left(\frac{d^2}{d\rho^2}+\frac{1}{\rho}\frac{d}{d\rho}-\frac{m^2}{\rho^2}\right)R_m + V(\rho)R_m = -E_n^b R_m, \qquad (2)$$

where μ is the in-plane reduced mass of the exciton, m and $R_m(\rho)$ are the exciton angular momentum and the in-plane wave function; $V(\rho)$ is the averaged in-plane image-charge-mediated potential given by

$$V(\rho) = \int dz_e \int dz_h |\psi^e(z_e)|^2 |\psi^h(z_h)|^2 V(z_e, z_h, \rho). \qquad (3)$$

Here $\psi^{e,h}(z)$ are the one-electron or hole wave functions for the direction perpendicular to the QW layers, and $V(z_e, z_h, \rho = |\rho_e - \rho_h|)$ is the electrostatic potential at point (ρ_e, z_e) caused by a hole at point (ρ_h, z_h).[16]

We have shown recently that the effective mass approximation is not valid for describing the motions of electrons and holes in the direction perpendicular to the QW layers;[19] this is quite reasonable because the well layers are composed of only one $[PbI_6]$ octahedron layer. Accordingly, the most reasonable wave functions $\psi^{e,h}(z)$ we should use to evaluate Eq. (3) are the highest occupied molecular orbital (HOMO) and the lowest unoccupied molecular orbital (LUMO) of a $[PbI_6]$ octahedron, which have been obtained by our first-

principle calculations.[20] However, to avoid tedious calculations, we used the simplest step functions $\psi^{e,h}=1/\sqrt{l_w}$ (in the well), 0 (outside the well), where l_w is the width of the well layer. In spite of this crude simplification, obtained results satisfactorily reproduce the experiment, as will be shown below. We used l_w and μ as adjustable parameters in the condition $l_w+l_b=(6.37+9.97)$ Å,[8] where l_b is the width of the barrier layer; and we set $\varepsilon_w=6.1$, $\varepsilon_b=2.1$, where ε_w and ε_b are the high-frequency dielectric constant of the well layer and the barrier layer, respectively. We also calculated the diamagnetic coefficient c_0 of the 1*s* excitons from their wave function Ψ with the formula $c_0=(e^2/8\mu)\langle\Psi|\rho^2|\Psi\rangle$ to fit the experimental data $[(2.6\pm0.1)\times10^{-7}$ eV/T$^2]$ obtained in our recent detailed magnetoabsorption study. The calculated E_1^b, E_2^b, E_3^b, E_4^b and c_0 were fitted to the experimental data.

We have obtained $E_1^b=362$ meV, $E_2^b=82$ meV, $E_3^b=32$ meV, $E_4^b=17$ meV, and $c_0=2.1\times10^{-7}$ eV/T^2 for $\mu=0.18m_0$, $l_w=6.0$ Å. The obtained in-plane Bohr radius of the 1*s* excitons is 14 Å. The obtained μ is slightly larger than that of the lowest-energy excitons in $(CH_3NH_3)PbI_3$ [$0.15m_0$ (Ref. 21)], which is reasonable because the reduction of dimensionality will result in the band narrowing, and thereby the larger reduced mass. The calculated resonance energies of the *ns* excitons are plotted as a function of $1/(n-1/2)^2$ by the crosses in Fig. 3. They quantitatively agree well with the experiment.

For comparison, the 1*s* excitons binding energy (for $\mu=0.18m_0$) are calculated to be 117 meV when the image charge effect is not included ($\varepsilon_b=\varepsilon_w=6.1$), which is about 2.4 times as large as the binding energy of the lowest-energy excitons in the three-dimensional (3D) analogue (bulk crystal), $(CH_3NH_3)PbI_3$ [50 meV (Ref. 21)]. Since the spatial confinement enhances the 1*s* excitons binding energy by a factor of 4 in the 2D limit, this enhancement factor 2.4 indicates that the spatial confinement for the 1*s* exciton is not sufficient. Nevertheless, it is worth noting that the 1*s* excitons binding energy (361 meV) is still at least 7 times larger than that in the 3D analogue $(CH_3NH_3)PbI_3$. The additional enhancement by a factor of $7/2.4=3$ is definitely due to the image charge effect, which is much larger than the image charge enhancement reported for the excitons in near-surface $In_xGa_{1-x}As/GaAs$QW.[4]

Figure 4 shows the calculated ρ dependence of the image-charge-mediated averaged potential $V(\rho)$ (solid line). Dotted line represents the ideal 2D Coulomb potential with a perfect image charge enhancement $V^{(2D)}(\rho)$.[22] The wave functions of the 1*s* and 2*s* excitons are represented by dashed-dotted lines. Although $V(\rho)$ agrees well with the ideal 2D Coulomb potential $V^{(2D)}(\rho)$ in the range $\rho>15$ Å, the former is shallower than the latter in the range $\rho<15$ Å owing to the weaker penetration of the lines of electric force. It follows that the *ns* ($n\geqslant2$) excitons form an ideal 2D hydrogenic series because their wave functions extend over the range $\rho>15$ Å, while the 1*s* exciton is deviated from it to the higher-energy side because the 1*s* excitons wave function occupies the inner region $\rho\leqslant15$ Å, where the image charge enhancement is not sufficient.

Observed relative oscillator strengths f_n/f_1, where f_n is the oscillator strength of the *ns* excitons, are summarized in Table I along with theoretical values. Here, the experimental f_n/f_1 was estimated using the following relation:

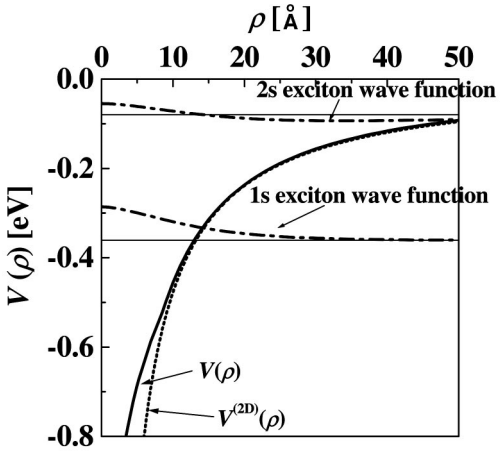

FIG. 4. Thick solid line shows the calculated averaged image-charge-mediated potential $V(\rho)$. Dotted line shows the ideal 2D Coulomb potential with a perfect image charge enhancement $V^{(2D)}\times(\rho)$. Dashed-dotted lines represent the wave functions of 1*s* and 2*s* excitons, and the corresponding energies are shown by thin solid lines.

$$f_n=\varepsilon_\infty\omega_{LT}m\omega_T V_0/2\pi e^2, \tag{4}$$

where m and e are the mass and the charge of the electron, respectively, ω_{LT} and ω_T frequencies of the LT splitting and the transverse exciton, respectively, V_0 the volume of the formula unit, ε_0 the average high-frequency dielectric constant.[7] The theoretical f_n/f_1 were calculated using the relation $f_n\propto|\Psi_n(0)|^2$,[23] where Ψ_n is the *ns* excitons wave functions which were obtained as eigenfunctions of Eq. (2). The experimental and calculated f_n/f_1 are in moderate agreement, while f_n/f_1 for the ideal 2D excitons do not reproduce the observed f_n/f_1 because f_1 is too large in the ideal 2D system. This confirms relatively insufficient enhancement for the 1*s* excitons in contrast to the *ns* ($n\geqslant2$) excitons.

B. Electric field effect

The EA spectra (Fig. 2) obtained in this study are qualitatively different from those under the electric field parallel to the QW layers[14] in that (1) the lifetime broadening observed in the 2*s* excitons under the electric field parallel to the QW layers is not seen for the perpendicular configuration

TABLE I. Experimental and theoretical relative oscillator strengths of *ns* excitons to that of 1*s* excitons, f_n/f_1. Theoretical f_n/f_1 values for an ideal 2D excitons system (Ref. 1) are also included.

	$n=1$	$n=2$	$n=3$	$n=4$
Observed	1	0.129	0.037	0.01(1)
Present model	1	0.21	0.056	0.023
Ideal 2D	1	0.037	0.008	0.003

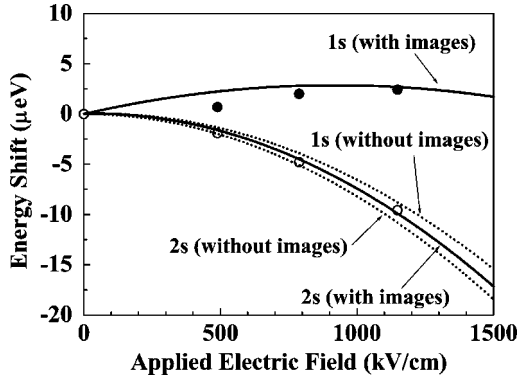

FIG. 5. Energy shifts of the 1*s* and 2*s* excitons peaks as functions of the applied electric field. Solid and open circles represent the experimental values for 1*s* and 2*s*, respectively, and the lines represent the theoretical shifts calculated with (solid line) and without (dashed line) the image charge effect.

even though the applied electric field is about 30 times larger. This is reasonable because the QW impede the 2*s* excitons ionization.[5] (2) The EA spectra show the redshift of the 2*s* excitons and the blueshift of the 1*s* excitons, because the EA spectra around the 1*s* excitons and the 2*s* excitons agree well in shape with the sign reversal of the first derivative, and the first derivative of the optical absorption spectrum, respectively. The measured shifts of the 1*s* and the 2*s* exciton peaks as a function of the electric field are shown by the solid and open circles in Fig. 5, respectively. Here magnitudes of the shifts ΔE were obtained using the relation $\Delta E=(\Delta\alpha L)(d\alpha L/dE)^{-1}$, where L is the sample thickness and E is the photon energy. The mechanism for the blueshift of the 1*s* excitons is as follows. Under electric field, the band-gap redshifts and the excitons binding energies are reduced by the same mechanism as conventional QCSE. The difference is that, in this crystal, the magnitude of the reduction in the 1*s* excitons binding energy ΔE_1^b exceeds that of the band gap.

To justify the mechanism stated above, we calculated the shifts of $E_1^{\rm res}$ and $E_2^{\rm res}$ under electric field in the following procedure: (i) We estimated the polarizability of the HOMO and the LUMO of the $[PbI_6]$ octahedron. The polarizability of the HOMO, α_S^H, was calculated by the *ab initio* molecular orbital calculations using the B-LYP method[24] and the CEP-31G basis sets.[25] We performed these calculations using the Gaussian 98 code,[26] and obtained $\alpha_S^H=36.5$ Å^3. For the polarizability of the LUMO, α_S^L, which cannot be calculated by the same code, we tentatively assume $\alpha_S^L\sim\alpha_S^H$, the validity of which will be confirmed later. (ii) Assuming that the electron/hole wave functions $\psi^{e,h}(z)$ are linear functions of z, slopes of which are chosen so that the induced polarizations are consistent with $\alpha_S^{H,L}F$, we calculated $V(\rho)$ using Eq. (3). (iii) We calculated E_1^b, E_2^b and their shifts (ΔE_1^b, ΔE_2^b) by solving Eq. (2). In this calculation, we neglected the self-energies of electron and hole that give only a minor contribution.[6]

The calculation showed that both E_1^b and E_2^b are reduced under electric fields, with the calculated $|\Delta E_1^b-\Delta E_2^b|$ nearly identical with the measured $|\Delta E_1^{\rm res}-\Delta E_2^{\rm res}|$, where $\Delta E_1^{\rm res}(>0)$ and $\Delta E_2^{\rm res}(<0)$ are the magnitude of the shifts of the 1*s* and 2*s* exciton resonance energy, respectively. ΔE_1^b is much larger than $\Delta E_2^b(\Delta E_1^b\sim 10\Delta E_2^b)$, which is quite reasonable because the 1*s* excitons have a smaller in-plane Bohr radius, and thus the field-induced separation of electron and hole has a larger influence on their binding energy. ΔE_2^b is much smaller than the magnitude of the measured 2*s* exciton shift, indicating that the observed energy shift of the 2*s* exciton is mainly due to that of the band gap. In other words, the mechanism of the energy shift of the 2*s* exciton is similar to the conventional QCSE. The magnitude of the band-gap shift is reasonable in the following order-of-magnitude arguments. The band-gap shift under the electric field F is given by $-(1/2)(\alpha_S^L-\alpha_S^H)F^2$; from the measured 2*s* exciton shift, we estimate $(\alpha_S^L-\alpha_S^H)\sim 1.5$ Å^3. Since the HOMO and LUMO of a $[PbI_6]$ octahedron is mainly composed of $Pb(6s)^2$ and $Pb(6s)(6p)$ respectively,[20] and their electron configuration is the same as the $6\,^1S_0$ and $6\,^3P_1$ state of Hg atoms, respectively, we believe that $(\alpha_S^L-\alpha_S^H)$ should be nearly equal to $\alpha_0(^3P_1)-\alpha_0(^1S_0)$, where $\alpha_0(^3P_1)$ and $\alpha_0(^1S_0)$ are the polarizabilities of the $6\,^1S_0$ and $6\,^3P_1$ state of Hg atoms, respectively. Since $(\alpha_S^L-\alpha_S^H)=1.5$ Å^3 and $\alpha_0(^3P_1)-\alpha_0(^1S_0)=3.95$ Å^3 (Ref. 27) are in the same order of magnitude, the magnitude of the measured band-gap shift is reasonable. Additionally, since $\alpha_S^L-\alpha_S^H\ll\alpha_S^H$, the validity of the relation $\alpha_S^L\sim\alpha_S^H$ assumed above is confirmed.

The solid and dashed lines in Fig. 5 show the theoretical electric-field dependence of the energy shifts of the exciton peaks, calculated with and without the image charge effect, respectively. Here we have determined the band-gap shifts so that the calculated $E_2^{\rm res}$ reproduce the measured $E_2^{\rm res}$. The measured shifts of $E_1^{\rm res}$ and $E_2^{\rm res}$ agree well with the theory only when the image charge effect is taken into account. Remarkable enhancement of ΔE_1^b is attributable to the smaller Bohr radius of the 1*s* excitons which is strongly reduced by the image charge effect. Note that the blueshift of the 1*s* excitons cannot be reproduced when the image charge effect is not taken into account. We thus conclude that the seemingly unusual blueshift of the 1*s* exciton is due to the large reduction of exciton binding energy exceeding that of the band gap, on which the image charge effect plays a significant role.

V. CONCLUSION

We have quantitatively shown that the *ns* ($n\geqslant 2$) excitons in $(C_6H_{13}NH_3)_2PbI_4$ form a nearly ideal 2D Wannier system where their binding energies are sufficiently enhanced by the 2D spatial confinement and image charge effect. Although these effects are relatively insufficient for the 1*s* exciton with smaller Bohr radius, its binding energy is still substantially enhanced. We have also demonstrated with calculations that the image charge effect plays a significant role in the unusual blueshift of the 1*s* exciton under the electric field.

ACKNOWLEDGMENTS

This work was supported by Core Research for Evolutional Science and Technology (CREST), Japan Science and Technology Corporation, Japan.

*Electronic address: tanaka@castle.t.u-tokyo.ac.jp

[1] M. Shinada and S. Sugano, J. Phys. Soc. Jpn. **21**, 1936 (1966).
[2] L. V. Keldysh, Pis'ma Zh. Eksp. Teor. Fiz. **29**, 716 (1979); JETP Lett. **29**, 658 (1979).
[3] E. Hanamura, N. Nagaosa, M. Kumagai, and T. Takagahara, Mater. Sci. Eng., B **1**, 255 (1988).
[4] L. V. Kulik, V. D. Kulakovskii, M. Bayer, A. Forchel, N. A. Gippius, and S. G. Tikhodeev, Phys. Rev. B **54**, R2335 (1996).
[5] D. A. B. Miller, D. S. Chemla, T. C. Damen, A. C. Gossard, W. Wiegmann, T. H. Wood, and C. A. Burrus, Phys. Rev. Lett. **53**, 2173 (1984).
[6] X. Zhang, Y. Li, X. Kong, and C. Wei, Phys. Rev. B **49**, 10432 (1994).
[7] T. Ishihara, J. Takahashi, and T. Goto, Phys. Rev. B **42**, 11099 (1990).
[8] T. Kataoka, T. Kondo, R. Ito, S. Sasaki, K. Uchida, and N. Miura, Phys. Rev. B **47**, 2010 (1993).
[9] T. Kondo, S. Iwamoto, S. Hayase, K. Tanaka, J. Ishi, M. Mizuno, K. Ema, and R. Ito, Solid State Commun. **105**, 503 (1998).
[10] J. Ishi, H. Kunugita, K. Ema, T. Ban, and T. Kondo, Phys. Rev. B **63**, 073303 (2001).
[11] J. Ishi, H. Kunugita, K. Ema, T. Ban, and T. Kondo, Appl. Phys. Lett. **77**, 3487 (2000).
[12] M. Era, S. Morimoto, T. Tsutsui, and S. Saito, Appl. Phys. Lett. **65**, 676 (1994).
[13] K. Shibuya, M. Koshimizu, Y. Takeoka, and K. Asai, Nucl. Instrum. Methods Phys. Res. B **194**, 207 (2002).
[14] K. Tanaka, F. Sano, T. Takahashi, T. Kondo, R. Ito, and K. Ema, Solid State Commun. **122**, 249 (2002).
[15] X. Hong, T. Ishihara, and A. V. Nurmikko, Phys. Rev. B **45**, 6961 (1992).
[16] E. A. Muljarov, S. G. Tikhodeev, N. A. Gippius, and T. Ishihara, Phys. Rev. B **51**, 14370 (1995).
[17] I. B. Koutselas, L. Ducasse, and G. C. Papavassiliou, J. Phys.: Condens. Matter **8**, 1217 (1996).
[18] G. M. Kavoulakis, Y. C. Chang, and G. Baym, Phys. Rev. B **55**, 7593 (1997).
[19] K. Tanaka and T. Kondo, Sci. Technol. Adv. Mater. **4**, 599 (2003).
[20] T. Umebayashi, K. Asai, T. Kondo, and A. Nakao, Phys. Rev. B **67**, 155405 (2003).
[21] K. Tanaka, T. Takahashi, T. Ban, T. Kondo, K. Uchida, and N. Miura, Solid State Commun. **127**, 619 (2003).
[22] The potential $V^{(2D)}$ is given by (Ref. 16) $V^{(2D)}(\rho) = -(e^2/\varepsilon^*\rho)$, $\varepsilon^* = \sqrt{\varepsilon_w \varepsilon_b [(\varepsilon_w l_w + \varepsilon_b l_b)/(\varepsilon_b l_w + \varepsilon_w l_b)]}$.
[23] P. Y. Yu and M. Cardona, *Fundamentals of Semiconductors*, 3rd ed. (Springer-Verlag, Berlin, Heidelberg, New York, 2001).
[24] A. D. Becke, Phys. Rev. A **38**, 3098 (1998).
[25] W. Stevens, H. Basch, and J. Krauss, J. Chem. Phys. **81**, 6026 (1984).
[26] M. J. Frisch *et al.*, Gaussian98, Revision A.7, Gaussian Inc., Pittsburgh, PA, 1998.
[27] D. M. Harber and M. V. Romalis, Phys. Rev. A **63**, 013402 (2000).